

Stress-Assisted Erosion of Poly(Glycerol-Co-Sebacate) Acrylate Elastomer

Nada Qari and Shengqiang Cai*

In this work, a systematic investigation is conducted on stress-assisted erosion of the photocurable and degradable elastomer poly(glycerol sebacate) acrylate (PGSA). Without external stress, it is confirmed that the elastomer undergoes surface erosion in an aqueous environment. Upon the application of mechanical stress, the results revealed that the surface erosion rate is dramatically accelerated. By studying the stress corrosion cracking (SCC) phenomena, it is demonstrated that the crack growth speed depends on the applied load and is significantly faster than the surface erosion rate of the elastomer. It is further shown that with decreasing the cross-link density of the elastomer, the crack growth speed during SCC can be slowed down due to the increased viscoelasticity of the material.

1. Introduction

Today, global consumption of plastics is greater than 200 million tons with an expected annual growth of 5%.[1] Yet, commonly used oil-based plastics such polystyrene (PS) and highdensity polyethylene (HDPE) do not undergo natural degradation that has significantly harmful effects on the environment. In fact, out of the 35.4 million tons of plastic that are generated each year in the United States, 26.8 million tons end up in landfills.^[2] While the overall number of recycled plastics remains relatively small with an 8.4% current recycling rate which is equivalent to 3 million tons per year. [2] Due to these facts, and in recent decades, the scientific community has rushed to the development of degradable polymers, which can undergo degradation in response to a trigger such as humidity, elevated temperatures, and light.[3,4] Since their development, degradable polymers have been used in surgery, drug delivery, tissue engineering, and the development of environmentally sustainable products.^[5,6-9] With the accelerated ongoing research efforts, degradable polymers are expected to rapidly replace nondegradable ones. In recent years, the sales of degradable polymers exceeded \$7 billion, accounting for almost 88% of the total biomaterial market.^[10] Future outlooks predict

N. Qari, S. Cai Program in Materials Science and Engineering University of California San Diego La Jolla, CA 92093, USA E-mail: shqcai@ucsd.edu

S. Cai
Department of Mechanical and Aerospace Engineering
University of California San Diego
La Jolla, CA 92093, USA

The ORCID identification number(s) for the author(s) of this article can be found under https://doi.org/10.1002/macp.202300268

DOI: 10.1002/macp.202300268

that the biocompatible materials market will reach \$11.9 billion suggesting a huge market for degradable polymers in the coming decades. [9,10]

Although polymer degradation is predominantly a chemical process, it is also accompanied by erosion where diffusion, dissociation, and other physical processes are involved. Degradation usually refers to the breakdown of certain bonds in the polymer's backbone. While erosion designates the loss of material from the bulk of the polymer in the form of oligomers and monomers.^[11]

When it comes to degradation mechanics, hydrolysis is the most common path taken by degradable polymers. Following the initial attack by water, there are a series of events, including a decrease in the molecular weight and a gradual loss of mechanical properties.^[12] After that, erosion, which is a predominantly physical process takes place and is typically characterized by the mass loss of a polymer matrix.[13] Polymer erosion can be divided into two types: bulk and surface erosion. When a polymer experiences bulk erosion, material is lost from the entire polymer volume. In this case, the erosion rate depends on the total amount of material and decreases as the material is depleted.^[14] On the other hand, when a polymer exhibits surface erosion, the material is lost from the polymer exterior surface. In this case, the erosion rate is directly proportional to the external surface area and the rate remains mostly constant until the polymer is completely eroded.[14] The kinetics of how a polymer degrades and erodes can significantly influence its performance along with the type of applications that it can be used for.

In addition to their degradation, the interaction between polymer chains with water can also lead to premature failure and crack growth. Due to the type of applications that degradable polymers are used in, they are often subject to various forces during degradation. However, according to our knowledge, many of the previous studies have ignored the effect of stress on the degradation process and most of them have been conducted using freestanding samples. Therefore, in this study, we aim to understand the influence of stress on polymer degradation from two perspectives. First, the effect of external stress and strain on the degradation process of a polymer without obvious defects. Second, the effect of stress and strain on the degradation of a polymer sample with a pre-crack. In fact, recent studies have shown that as polymers start to degrade, cracks and voids will begin to form.^[5,11] We believe that in the presence of an external load, the applied stress will be concentrated at the tip of the crack and since the polymer is undergoing degradation due to its interaction with water, the concentrated stress will lead to crack growth and eventual failure of the material.^[5] This type of phenomenon has been observed www.advancedsciencenews.com

www.mcp-journal.de

in many materials including metals, natural rubber, and nondegradable polymers, and is known as stress corrosion cracking (SCC).[5,15-18]

In the case of degradable polymers such as poly(glycerol sebacate) (PGS), water from the environment reacts with the ester bond on the polymer backbone resulting in the formation of carboxyl and hydroxyl groups.^[4] These reactions break the chain and degrade the polymer. As the polymer degrades, its mechanical properties or size may change and so will its performance within a specific application, especially in the presence of an external load. In fact, recent studies have shown that the speed of the hydrolytic crack depends on relative humidity, pH, and applied load. [4,5,19]

The degradation of PGS along with its biocompatibility under physiological conditions is also one of its greatest advantages allowing it to be used for the development of many biomedical applications such as scaffolds, membranes, and drug delivery systems. [20] Although the deterioration of its mechanical properties as a function of degradation has hindered its progress, recent studies have been able to overcome these obstacles through te chemical functionalization of the polymer's backbone.[20,21]

In recent years, the acrylated derivative of PGS known as poly(glycerol sebacate) acrylate (PGSA) has sparked a lot of interest within the research community. When compared to PGS, PGSA is a strong, stretchable, and photocurable elastomer that can be easily crosslinked in the presence of ultraviolet radiation.^[5,22] This makes it possible to process solid PGSA structures using bioprinting along with various types of lightbased lithography. Because of its practical processing techniques, PGSA has been used to develop degradable stents and porous capsules for drug delivery. [22,23]

In this work, we conduct a detailed investigation of PGSA with the aspiration of understanding its hydrolytic degradation kinetics and how the degradation rate of a sample without obvious defects changes with the applied strain. Furthermore, to study the coupled effect of degradation and external mechanical loading, we systematically studied the SCC phenomena using PGSA samples with pre-cut and two different crosslink densities.

By studying the degradation of PGSA at high pH and in the absence of external stress, we confirmed that the polymer undergoes surface erosion with an observable erosion front. By investigating the degradation kinetics of PGSA at neutral pH and under varying stresses and strains, we observed that the degradation rate is accelerated when stresses and strains are applied to the degrading sample. Finally, we investigated the coupled effects of degradation and mechanical loading on PGSA through our study of the SCC phenomena. In doing so, our results have revealed that crack growth outruns PGSA's surface erosion rate which is consistent with recent studies that have reported similar behavior in other types of degradable polymers.^[5]

2. Experimental Section

2.1. Chemical Synthesis

2.1.1. Polycondensation of PGS Prepolymer

The synthesis of the PGS and PGSA polymers were prepared by following previous articles.[22-24] Briefly, in a three-neck round boiling flask, the pre-polymer PGS was prepared through the polycondensation reaction of an equimolar ratio of viscous glycerol (27.6 g; Sigma-Aldrich G5516) and solid sebacic acid pellets (60.6 g; Sigma-Aldrich 283 258) at the temperature of 140 °C, under inert N₂ atmosphere for 1 h. Once the solid sebacic acid pellets were fully dissolved within the viscous glycerol, the temperature was reduced to 120 °C, the flow of N2 was stopped and the pressure was reduced to 15 mbar for 48 h (Figure 1a). Upon completion, the highly viscous PGS prepolymer was collected and stored in brown glass vials at -4 °C in preparation for the acrylation step.

2.1.2. Acrylation of PGS Prepolymer

The solid PGS prepolymer (30 g) was defrosted at 50 °C by placing the storing vial in a water bath for 30 min. The defrosted viscous PGS prepolymer was carefully poured into a three-neck round boiling flask and dissolved in dichloromethane (300 mL; Sigma-Aldrich 75-09-2). After that, acryloyl chloride (2.75 mL, Sigma-Aldrich A24109) was added to the reaction flask (Figure 1b) with the purpose of converting the OH groups of PGS to acrylate groups (Figure 1c). Additionally, triethylamine (4.50 mL, Sigma-Aldrich 121-44-8) was added to neutralize the reaction and entrap the HCl by-product in the form of white salt that was filtered out of the reaction through vacuum filtration after 24 h. At this stage, the reaction mixture contains the acrylated PGS polymer along with the DCM solvent where a rotary evaporator was used to remove approximately 93% of the remaining solvent (279 mL). The final low-viscosity PGSA polymer solution (18 vol.% solvent) was collected and stored in brown vials at −4 °C for future usage.

2.2. Cross-Linking Step

To prepare solid samples, PGSA polymer solution (5.15 g) was mixed with 2-hydroxy-2-methylpropiophenone (HMPP, 0.105 g, Sigma-Aldrich 405 655), a photo-initiator, and cross-linked under ultraviolet radiation (UV) via free radical polymerization through the acrylate groups (Figure 1d). To ensure complete solvent evaporation, cross-linked PGSA samples were left to dry on the bench for 1 h before conducting any type of testing or characterization.

2.3. NMR Characterization

To confirm the successful conversion of the PGS prepolymer OH groups to acrylate groups, an NMR test was conducted using the spectrometer (Jeol 500 ECA 500) and the 1H-proton spectra were collected for PGS and PGSA.

As shown in Figure 2a, the PGS prepolymer spectrum showed five distinct peaks that represented the prepolymer's different protons. The peak that appears at 7.25 ppm belonged to chloroform-D, which was the solvent used to dissolve the polymer in preparation for NMR testing.

The same spectrum was collected for the PGSA polymer, where three new distinct peaks appeared between 5.5 and 6.5 ppm as a result of the acrylation reaction (Figure 2b). Also, it is important to note that two new sharp peaks appeared between 1 and 2 ppm which arose due to presence of 18 vol.% solvent in the final product as previously discussed in section 2.1.2.

15213935, 2024, 4, Downloaded from https://onlinelibrary.wiely.com/doi/10.1002/map.202300268 by University Of California San Diego, Wiley Online Library on [11/02/2025]. See the Terms and Conditions (https://onlinelibrary.wiely.com/terms-and-conditions) on Wiley Online Library for rules of use; OA articles are governed by the applicable Creative Commons License

15213935, 2024, 4, Downloaded from https://onlinelibrary.wiley.com/doi/10.1002/macp.202300268 by University Of California San Diego, Wiley Online Library on [11/02/2025]. See the Terms and Conditions (https://onlinelibrary.wiley.com/doi/10.1002/macp.202300268 by University Of California San Diego, Wiley Online Library on [11/02/2025]. See the Terms and Conditions (https://onlinelibrary.wiley.com/doi/10.1002/macp.202300268 by University Of California San Diego, Wiley Online Library on [11/02/2025]. See the Terms and Conditions (https://onlinelibrary.wiley.com/doi/10.1002/macp.202300268 by University Of California San Diego, Wiley Online Library on [11/02/2025]. See the Terms and Conditions (https://onlinelibrary.wiley.com/doi/10.1002/macp.202300268 by University Of California San Diego, Wiley Online Library on [11/02/2025]. See the Terms and Conditions (https://onlinelibrary.wiley.com/doi/10.1002/macp.202300268 by University Of California San Diego, Wiley Online Library on [11/02/2025]. See the Terms and Conditions (https://onlinelibrary.wiley.com/doi/10.1002/macp.202300268 by University Of California San Diego, Wiley Online Library.

conditions) on Wiley Online Library for rules of use; OA articles are governed by the applicable Creative Commons I

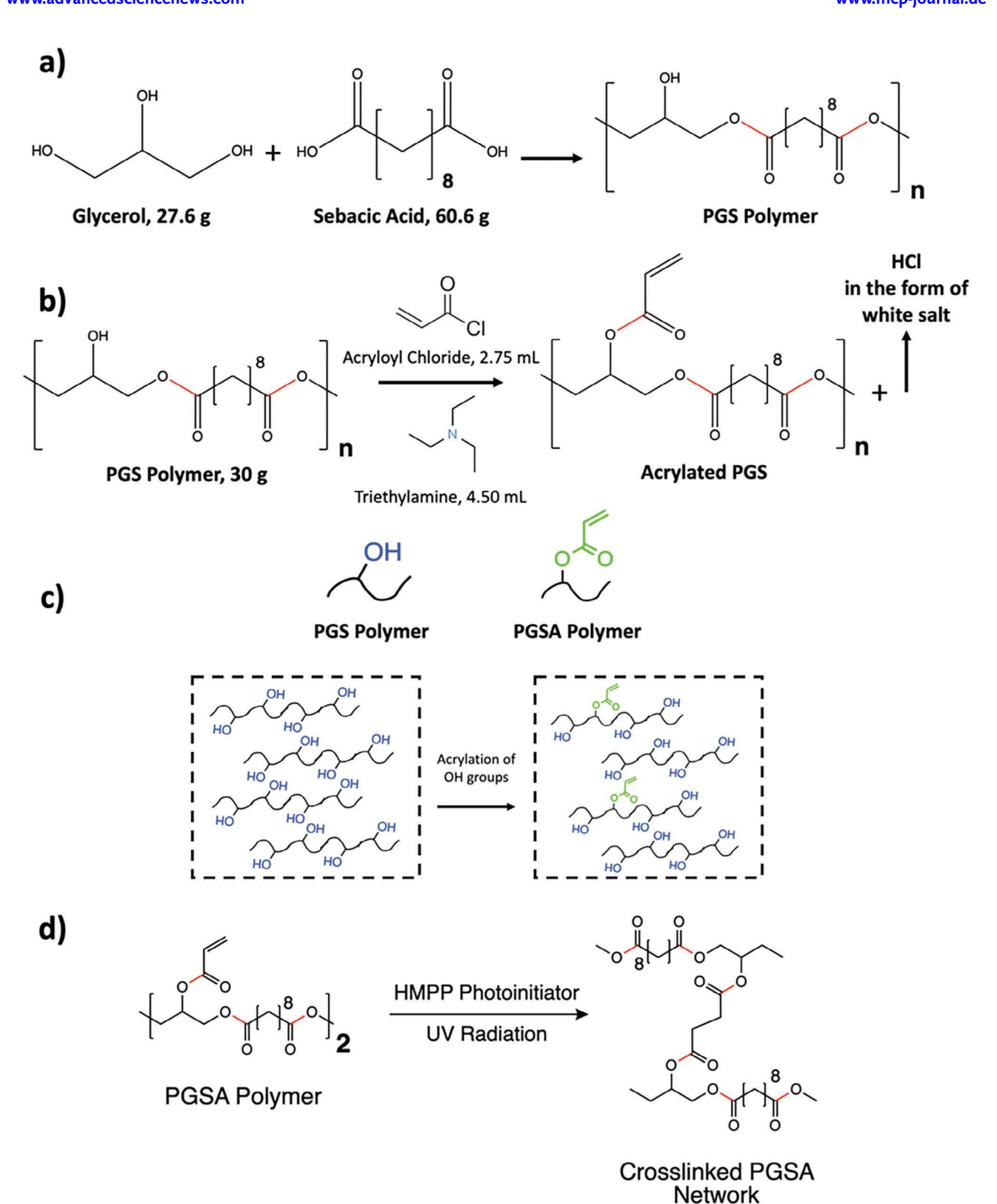


Figure 1. The first step of synthesizing the PGSA polymer involves the condensation of glycerol and sebacic acid at 120 °C and 15 mbar for 48 h which results in the formation of the PGS pre-polymer (a). The PGS is reacted with acryloyl chloride in an acid-base reaction neutralized by triethylamine to generate the PGSA polymer while the HCl byproduct is filtered out of the reaction in the form of white salt (b). The acrylation reaction converts the OH groups to acrylate groups and the desired PGSA polymer is obtained (c). The PGSA polymer is crosslinked using 2-Hydroxy-2-methylpropiophenone (HMPP) photoinitiator through the acrylate group via free radical polymerization in the presence of UV radiation (d).

15213935, 2024. 4, Downloaded from https://onlinelibrary.wiley.com/doi/10.1002/macp.202300268 by University Of California San Diego, Wiley Online Library on [11/02/2025]. See the Terms and Conditions (https://onlinelibrary.wiley.com/term

) on Wiley Online Library for rules of use; OA articles are governed by the applicable Creative Commons

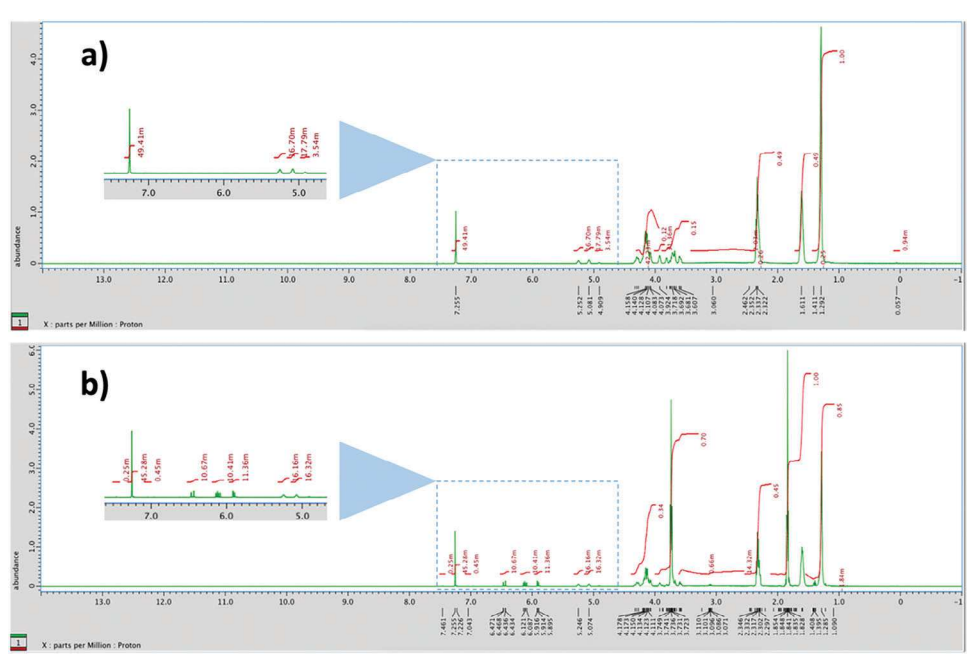


Figure 2. The proton NMR spectrum of the PGS prepolymer (a) and PGSA polymer (b) where the region from 5 to 7 ppm is added to each spectrum as an inset for comparison purposes and to illustrate the successful acrylation of the PGS prepolymer.

3. Results and Discussion

3.1. The Degradation of PGSA

3.1.1. Demonstration of Surface Erosion of PGSA in a High pH Aqueous Environment

Like PGS, the ester bonds present in PGSA undergo hydrolytic degradation in the presence of water which results in breaking down the polymer chain into its alcohol and carboxylic acid derivatives (**Figure 3**). To determine the degradation mechanism of PGSA and whether it undergoes surface or bulk erosion, we investigate the in-situ degradation of PGSA in a stress-free high pH environment.

This was achieved by preparing a cylindrical-shaped sample with the dimensions shown in **Figure 4a** where each side of the sample was exposed to 10 min of UV radiation to complete the crosslinking reaction. Additionally, the sample was dyed red using Rhodamine B (0.0035 g, Acros-Organics 25GRR) to allow clear observation of the erosion process.

To accelerate the degradation process so that it is observable within a few hours, the crosslinked sample was fully immersed in a 0.5 (M) NaOH solution where the pH was equal to 13.69. This setup was placed under an optical microscope and the degradation reaction was observed from a top-down view (Figure 4a). Throughout the experiment, and using the microscope's camera, we capture an image every 10 minutes until the degradation reaction was complete with no sample left in the reaction flask.

As seen from the images in Figure 4b, at time = 0 min, the diameter is equal to 7.8 mm. Within the first 10 min, the diameter reduces to 7.4 mm in addition to the appearance of a yellow ring around the sample's diameter which is associated with the diffusion of the dyes from the sample to the external solution. The erosion of the sample is illustrated by the images captured at time = 190, 320, and 400 min. Finally, after 7.6 h, the sample was fully degraded, and no more mass was left in the reaction flask.

The data collected throughout the experiment were used to plot the diameter as a function of time (Figure 4c) and by measuring the slope through linear fitting (illustrated by the dashed

Figure 3. When placed in an aqueous solution, the PGSA ester bonds (illustrated in red) undergo hydrolytic degradation where they break down to the alcohol and carboxylic acid derivatives.

15213935, 2024, 4, Downloaded from https://onlinelibrary.wiley.com/doi/10.1002/map.202300268 by University Of California San Diego, Wiley Online Library on [11/02/2025]. See the Terms

) on Wiley Online Library for rules of use; OA articles are governed by the applicable Creative Commons

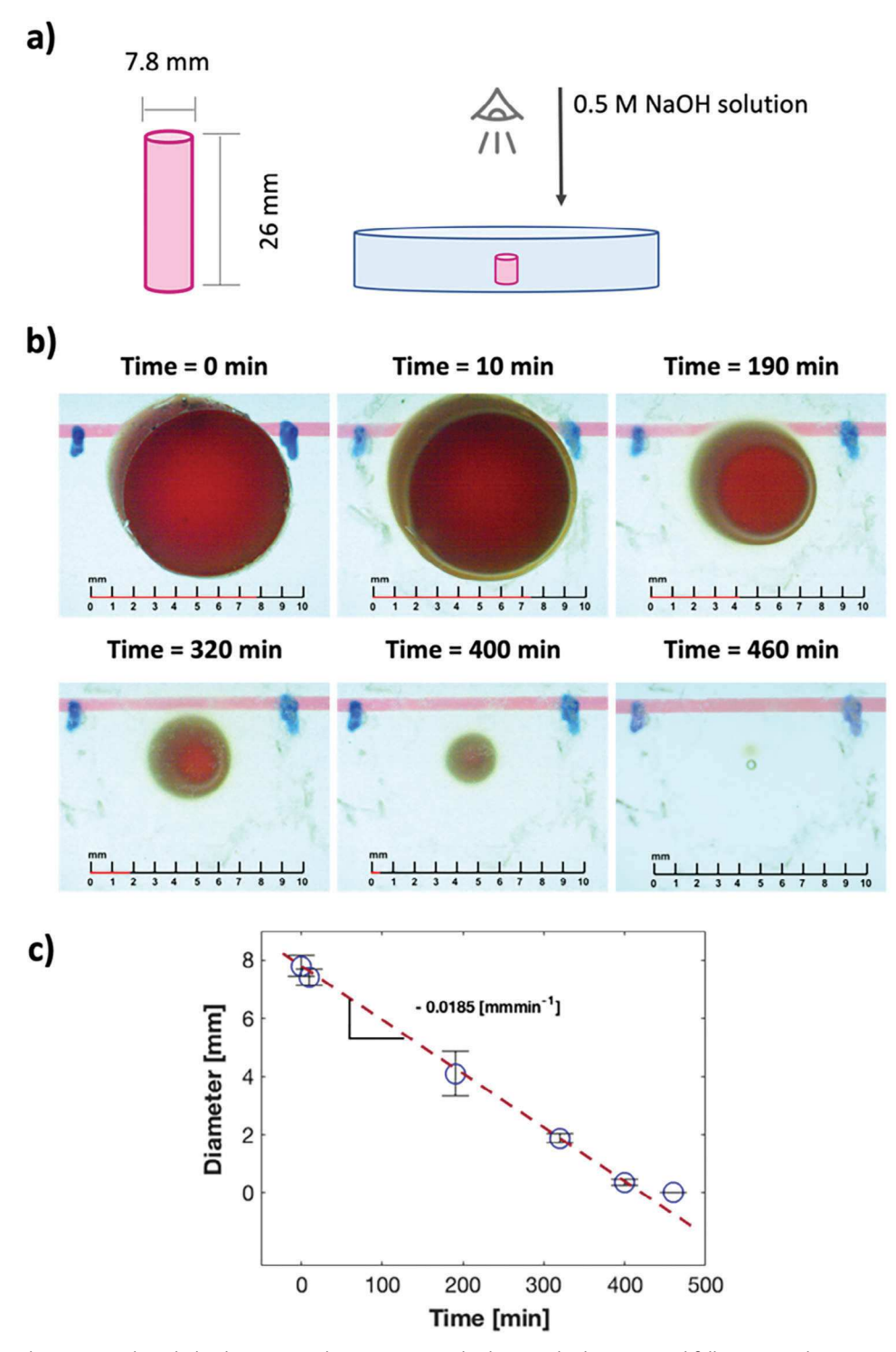


Figure 4. A cylindrical PGSA sample with the dimensions shown in (a) was dyed using Rhodamine B and fully immersed in a 0.5 M NaOH solution (pH 13.69) where the surface erosion was observed in real-time using an optical microscope with a top-down view. Images were captured every 10 min for 7.6 h where the main stages of degradation are highlighted in (b). The experimental images were used to measure the cylinder's diameter and how it changes as a function of time at t = 0, 10, 190, 320, 400, and 460 min, respectively. The results were plotted as a function of time where linear fitting illustrated by the dashed line was used to determine the degradation rate at pH 13.69 that was equal to 0.0185 mm min⁻¹ (c). The error bars represent the standard deviations calculated based on three replicate samples for each data point shown in (c).

15213935, 2024, 4, Downloaded from https://onlinelibrary.wiley.com/doi/10.1002/macp.20200208 by University Of California San Diego, Wiley Online Library on [1/10/2025]. See the Terms and Conditions (https://onlinelibrary.wiley.com/terms

and-conditions) on Wiley Online Library for rules of use; OA articles are governed by the applicable Creative Commons

line), we find that the degradation speed of PGSA in such conditions is equal to 0.0185 mm min $^{-1}$. Additionally, our results confirm that surface erosion is the dominant degradation mechanism for free standing PGSA. Furthermore, recently published in-situ degradation experiments of PGSA under similar conditions (0.2 $\,\mathrm{M}$ NaOH) confirm that mass change as a function of degradation time also follows a linear trend. [25–27] We find that these degradation trends are consistent with what we observed when monitoring the diameter change as a function of time, despite the difference in the measured physical parameters.

3.1.2. Demonstration of the Effect of Mechanical Stress on the Hydrolytic Rate of PGSA

To directly observe the effect of stress on the hydrolysis of PGSA, we designed a T-shaped PGSA sample with the dimensions illustrated in **Figure 5a**. This sample was placed on a linear actuator that was used to apply a 25% elongation on the entire sample where the applied elongation was held constant for the total duration of the experiment (7 days) (Figure 5b). This geometry was selected so that the stretched sample can experience two different stresses under the same force due to the difference in cross-sectional area. The wide region (20 mm \times 0.93 mm) would experience lower stress since it has a larger cross-sectional area whereas the narrow region (10 mm \times 0.93 mm) would experience higher stress.

To study the stress-assisted hydrolysis, the stretched sample was fully immersed in a water tank (pH 7) and the thickness of both the wide and narrow regions were measured daily. As a control test, a PGSA sample was placed in a water medium with no applied stress for 10 days where the thickness was measured every 2 days. The thickness data collected throughout the experiment were plotted as a function of time where we can clearly observe the effect of stress on the degradation rate (Figure 5c).

At neutral pH and with no applied stress, the PGSA degradation rate is approximately 0.0083 mm d^{-1} . However, when the sample is stretched under the same pH conditions, the wide region experiences a 0.076 mm d^{-1} degradation rate (89% faster than the control test). Whereas the narrow region degrades at a rate of 0.119 mm d^{-1} which is 93% faster than the control test. Based on the results reported in Figure 5, we were able to show that there is a direct relationship between the degradation rate of PGSA and the applied stress where our results confirm that with higher stress, the PGSA polymer degrades faster.

3.1.3. Quantitative Effect of Applied Strain on the Surface Erosion Rate of PGSA

To study the effect of applied strain systematically and more quantitatively on the hydrolysis-induced surface erosion of PGSA, we conducted further experiments using a homogeneous sample with the dimensions shown in **Figure 6**a. A linear actuator was used to stretch the sample where the applied strain was held constant for 7 days (Figure 6b). Likewise, the stretched sample was fully immersed in a water tank with pH 7 and the thickness was measured daily.

This setup was used to investigate the effect of six differently applied strains starting with 5% followed by 10%, 15%, 20%,

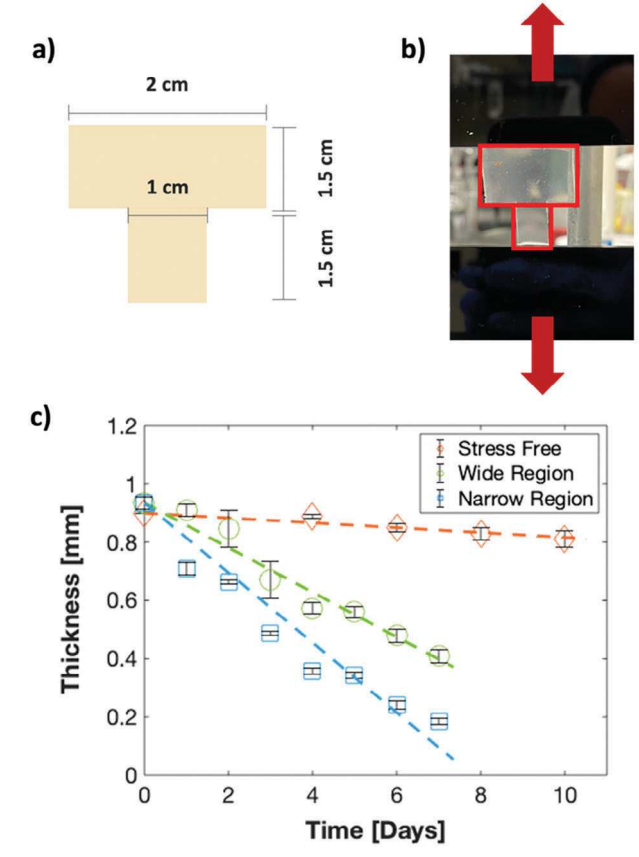


Figure 5. To determine the effect of stress on the surface erosion of PGSA, we designed a T-shaped PGSA sample with the dimensions shown in (a) and used a linear actuator to stretch the sample by 25% where the stretch was held constant (b). The stretched sample was placed in a water tank (pH 7) while monitoring the thickness every day for 1 week for both the wide and narrow regions of the T-shaped structure. Upon completion, the collected thickness values were plotted as a function of time where the error bars illustrate the standard deviation values based on 3 replicate tests (c). Our experimental results along with linear fitting shown as dashed lines confirm that the narrow region degrades faster than the wide region. Furthermore, when compared to an unstretched sample that is exposed to the same pH conditions, we confirmed that the stretched PGSA degrades at a faster rate.

25%, and 30%, respectively. As a reference state, a PGSA sample was placed in a water medium with no applied strain for 10 days where the thickness was measured every 2 days. The data collected throughout the experiment were plotted as a function of time where a clear dependence between the applied strain and degradation rate can be observed (Figure 6c).

At neutral pH and with no applied strain, the PGSA sample degrades at a slow rate of 0.0083 mm d $^{-1}$. At 5% strain, the degradation rate is increased to 0.034 mm d $^{-1}$. The application of 10% strain on the sample further increases the degradation rate to 0.048 mm d $^{-1}$. When a 15% strain is applied to the sample, the degradation rate goes up to 0.076 mm d $^{-1}$. At 20% and 25% strain, the degradation rates are \approx 0.0946 and 0.0941 mm d $^{-1}$, respectively. However, when a 30% strain is applied to the sample, the degradation rate increases to 0.116 mm d $^{-1}$. Based on that, our results confirm the relationship between applied strain and

15213935, 2024, 4, Downloaded from https://onlinelibrary.wiley.com/doi/10.1002/macp.202020268 by University Of California San Diego, Wiley Online Library on [1/10/2025]. See the Terms and Conditions (https://onlinelibrary.wiley.com/terms/

and-conditions) on Wiley Online Library for rules of use; OA articles are governed by the applicable Creative Commons

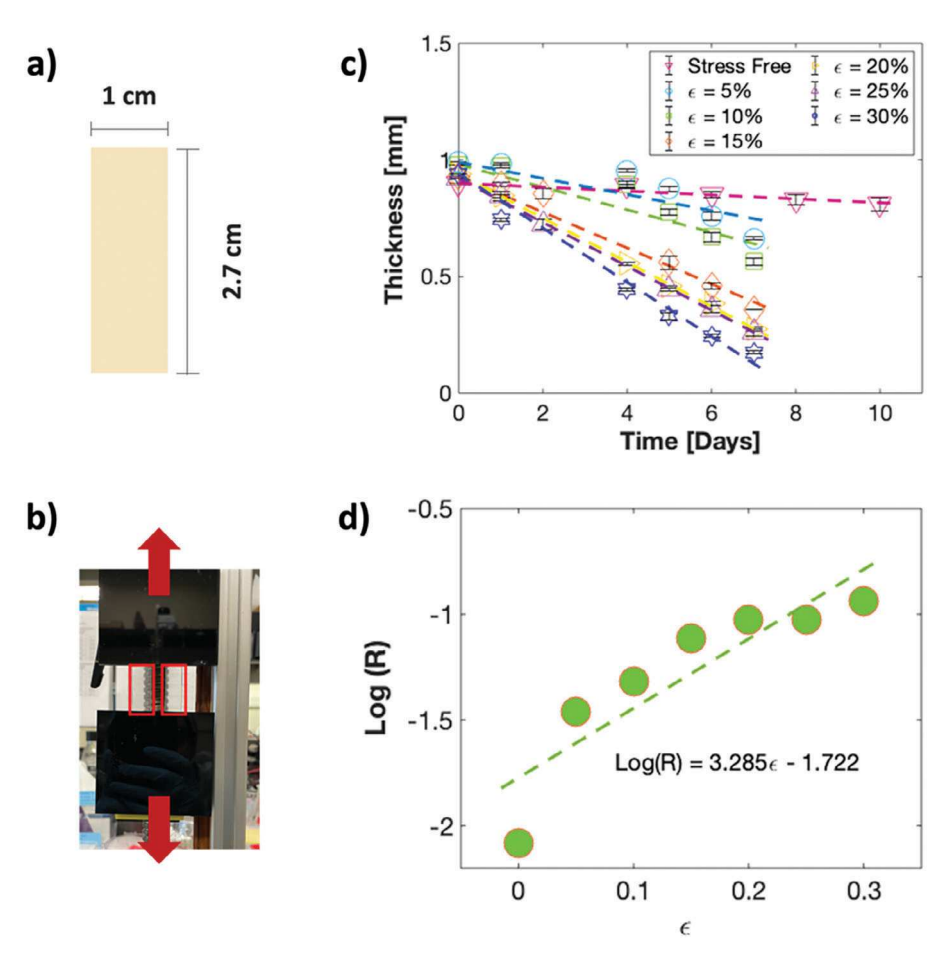


Figure 6. To determine the effect of strain on surface erosion, we designed a tensile-shaped PGSA sample with the dimensions shown in (a) and used a linear actuator to apply 6 different strains starting from 5% followed by 10%, 15% 20%, 25%, and 30% respectively (b). A freshly prepared sample with the same geometry was used for each test illustrated in (b). The stretched samples were placed in a water tank (pH 7) where the thickness was monitored every day for 1 week. Upon completion, the thicknesses were plotted as a function of time where we observed an increase in the degradation rate at higher strain. Error bars were used to represent the standard deviation values based on three replicate tests in (c). Linear fitting illustrated by dashed lines was used to determine the different degradation rate (R) values in mm d⁻¹ (c). The logarithmic values of (R) were determined and plotted as a function of the applied strain in (d) where linear fitting indicated by the dashed line was used to calculate the slop and y-intercept highlighted by the equation in (d).

degradation rate (*R*) where the rate is dramatically increased at higher strain. To further illustrate this effect, Figure 6d plots the logarithmic values of the degradation rate (*R*) as a function of the applied strain.

3.2. Stress Corrosion Cracking

Previous studies have shown that if pre-cracks exist in degradable polymers, the stress corrosion cracking may outrun the degradation process because the stress can be highly concentrated near the crack tip. So, next, we study the stress corrosion cracking (SCC) process of PGSA.

3.2.1. Effect of Cross-Link Density on the Mechanical Behavior of PGSA

As mentioned previously and when compared to the PGS elastomer, one advantage of using acrylated PGS is its photocurable

properties. The crosslinking mechanism mentioned in Section 2 (Figure 1d) allows us to control the crosslink density simply by adjusting the polymer's exposure time to UV radiation. And by changing the crosslink density, we can alter the mechanical properties of the PGSA polymer.

To gain deeper insight into how UV exposure time influences the mechanical properties of PGSA, we summarize the results in Table 1 where the distinction between the two samples becomes apparent. For example, the ultimate tensile strength obtained from Figure 7a shows that the strength is increased by 122% as result of increased UV exposure time.

Furthermore, and since pure shear geometry is adopted to complete the stress corrosion cracking experiment, the shear modulus (μ) can be used to quantitatively evaluate the change in crosslink density based on the following equation:

$$\mu = 4Nk_BT \tag{1}$$

15213935, 2024, 4, Downloaded from https://onlinelibrary.wiley.com/doi/10.1002/macp.202300268 by University Of California San Diego, Wiley Online Library on [11/02/2025]. See the Terms and Conditions (https://onlinelibrary.wiley.com/doi/10.1002/macp.202300268 by University Of California San Diego, Wiley Online Library on [11/02/2025]. See the Terms and Conditions (https://onlinelibrary.wiley.com/doi/10.1002/macp.202300268 by University Of California San Diego, Wiley Online Library on [11/02/2025]. See the Terms and Conditions (https://onlinelibrary.wiley.com/doi/10.1002/macp.202300268 by University Of California San Diego, Wiley Online Library on [11/02/2025]. See the Terms and Conditions (https://onlinelibrary.wiley.com/doi/10.1002/macp.202300268 by University Of California San Diego, Wiley Online Library on [11/02/2025]. See the Terms and Conditions (https://onlinelibrary.wiley.com/doi/10.1002/macp.202300268 by University Of California San Diego, Wiley Online Library on [11/02/2025]. See the Terms and Conditions (https://onlinelibrary.wiley.com/doi/10.1002/macp.202300268 by University Of California San Diego, Wiley Online Library on [11/02/2025]. See the Terms and Conditions (https://onlinelibrary.wiley.com/doi/10.1002/macp.202300268 by University Of California San Diego, Wiley Online Library on [11/02/2025]. See the Terms and Conditions (https://onlinelibrary.wiley.com/doi/10.1002/macp.202300268 by University Of California San Diego, Wiley Online Library on [11/02/2025]. See the Terms and Conditions (https://onlinelibrary.wiley.com/doi/10.1002/macp.202300268 by University Of California San Diego, Wiley Online Library on [11/02/2025]. See the Terms and Conditions (https://onlinelibrary.wiley.com/doi/10.1002/macp.202300268 by University Of California San Diego, Wiley Online Library on [11/02/2025]. See the Terms and Conditions (https://onlinelibrary.wiley.com/doi/10.1002/macp.202300268 by University Of California San Diego, Online Diego, Online Diego, Online Diego, Online Diego, Online Diego, Online Diego, Onl

onditions) on Wiley Online Library for rules of use; OA articles are governed by the applicable Creative Commons License

Table 1. The mechanical properties of PGSA samples with varying crosslink densities and geometries based on UV exposure time along with standard deviation values based on 3 tested samples.

Pure shear – Un-notched					
5 min of UV Exposure	15 s of UV Exposure				
28.80 ± 0.72	33.70 ± 2.85				
36.40 ± 3.29	16.36 ± 2.07				
134 ± 22	47 ± 2				
$6.67 \times 10^3 \pm 547.94$	$2.93 \times 10^3 \pm 415.40$				
	5 min of UV Exposure 28.80 ± 0.72 36.40 ± 3.29 134 ± 22				

Pure shear – Notched				
Mechanical property	5 min of UV Exposure	15 s of UV Exposure		
Fracture strain [%]	16.30 ± 1.91	22.52 ± 4.37		
Ultimate tensile strength [kPa]	21.73 ± 2.76	12.19 ± 1.28		
Fracture toughness [J m ⁻²]	19.56 ± 6.58	14.79 ± 4.07		

where *N* is the number of chains per unit volume, K_B is Boltzmann's constant (1.38×10⁻²³ J K⁻¹), and *T* is the absolute temperature (300 K). From Table 1, the shear moduli for the high and low crosslink density samples are equal to 134 kPa and 47 kPa,

respectively. By using Equation 1, we find that the value of N is increased from $2.83 \times 10^{24} \text{ m}^{-3}$ to $8.09 \times 10^{24} \text{ m}^{-3}$ when the PGSA sample is exposed to 5 minutes of UV. By simply increasing the sample's UV exposure time from 15 s to 5 min, the number of chains per unit volume is increased by 185% that confirms the change in cross-link density as a function of UV exposure time.

To determine the fracture toughness of PGSA and how it changes as a function of cross-link density, we conducted tensile testing at 0.25% s⁻¹ strain rate using pure shear geometry (50 mm \times 10 mm \times 1 mm). When the samples are un-notched, calculating the area under the stress-strain curve allows us to determine the work of rupture W in J m⁻³ (Figure 7a). By doing so, we find that high crosslink density PGSA has a $W = 6.67 \times 10^3$ J m⁻³ while low crosslink density PGSA has a W that is equal to 2.93×10^3 J m⁻³ (Table 1).

By conducting the same type of tensile testing using notched samples with pure shear geometry, we can determine the critical strain $\epsilon_{critical}$ and how it changes as a function of crosslink density. As seen from Figure 7b and Table 1, high cross-link density PGSA fractures at $\epsilon_{critical}=16.30\%$ while low crosslink density PGSA fractures at $\epsilon_{critical}=22.52\%$. By determining the values of both the work of rupture and the critical strain, we can determine the fracture toughness Γ in J m⁻² for each type of PGSA using Equation 2:

$$\Gamma = HW\left(\varepsilon_{critical}\right) \tag{2}$$

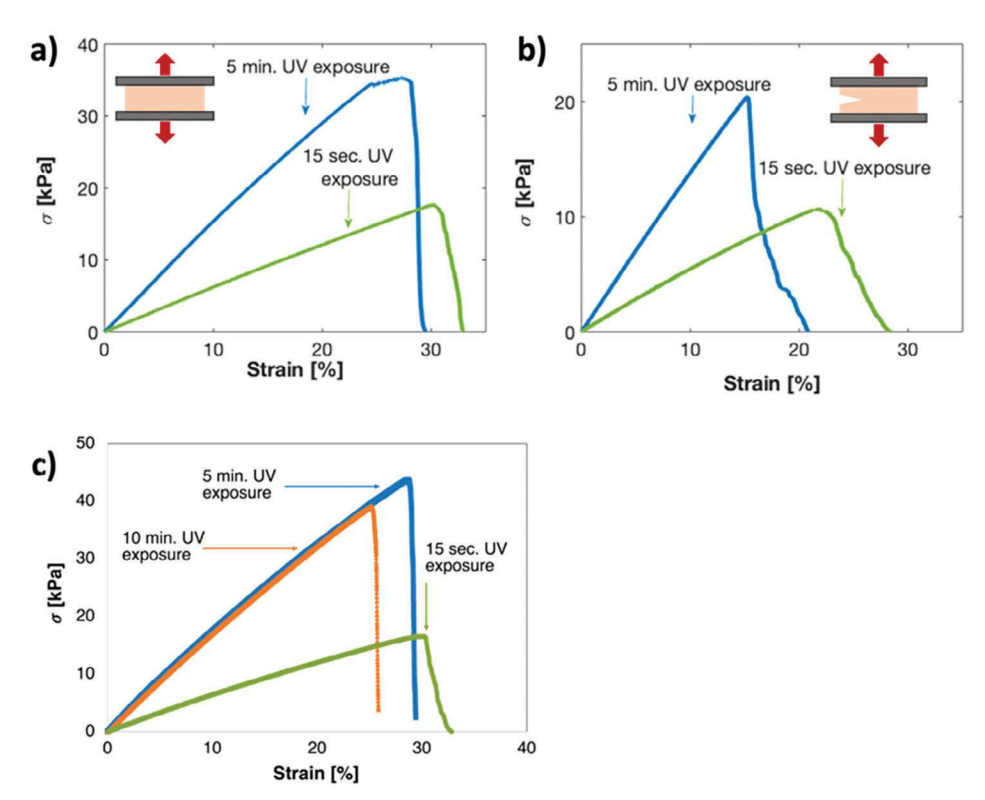


Figure 7. To calculate the work of rupture, we tested both types of PGSA samples with un-notched pure shear geometry and used the plot to determine the area under the curve (a). To determine the value of the critical strain along with the range of energy release rate values that can be used in the stress corrosion cracking experiment, we tested both types of PGSA samples with notched pure shear geometry (b). Using the same pure shear geometry and by applying a tensile force at 0.25% s⁻¹, we confirmed that the mechanical properties of PGSA exhibit minimal change when exposed to more than 5 min of UV radiation (c). All of the plotted figures were generated using mean values where the standard deviations are reported in Table 1 based on three tested samples for each geometry using both types of PGSA.

15213935, 2024, 4, Downloaded from https://onlinelibrary.wiley.com/doi/10.1002/macp.202020268 by University Of California San Diego, Wiley Online Library on [1/10/2025]. See the Terms and Conditions (https://onlinelibrary.wiley.com/terms/

conditions) on Wiley Online Library for rules of use; OA articles are governed by the applicable Creative Commons

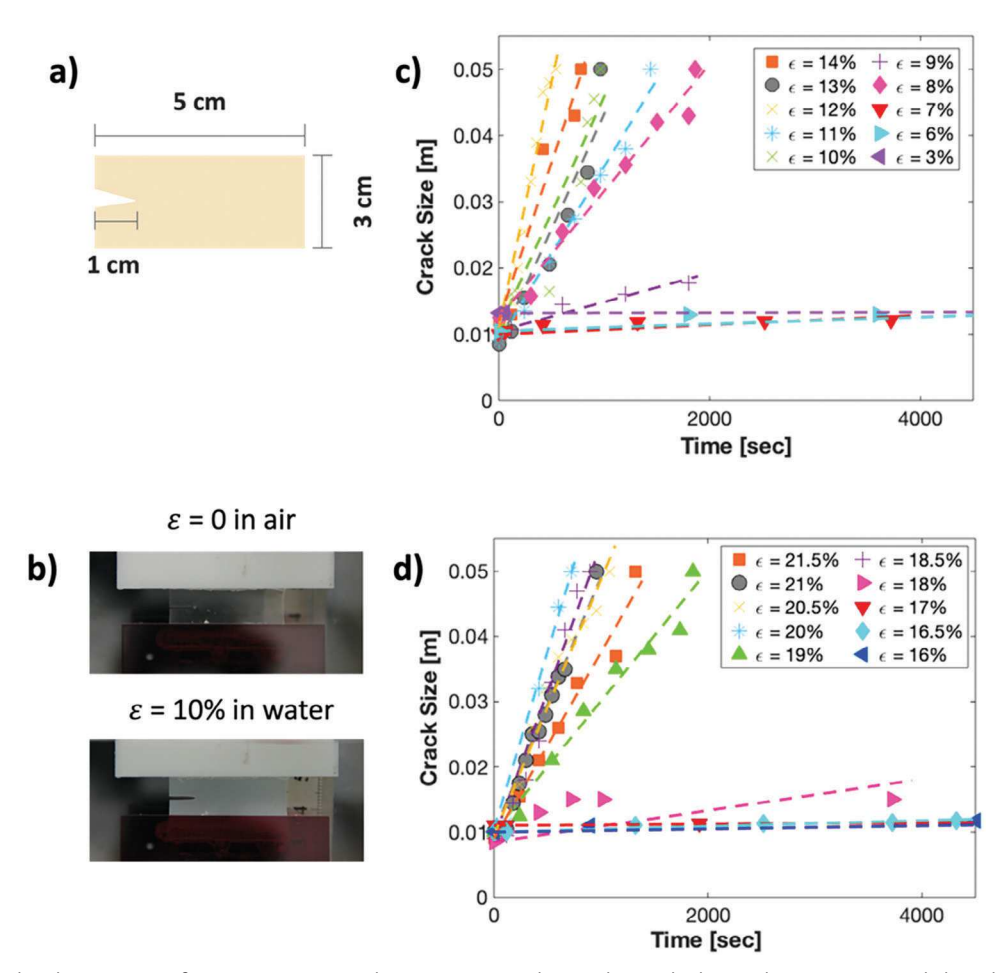


Figure 8. To study the phenomenon of stress corrosion cracking in PGSA, we designed a notched pure shear testing sample based on the dimensions shown in (a). The sample was attached to the Instron machine using an in-house designed water tank setup (b). The 10 N load cell was used to apply a specified strain which was held constant until fracture while the sample was fully immersed in DI water at neutral pH (b). Throughout each experiment, a camera setup was used to consistently capture images to determine the crack size growth rate as a function of time. The PGSA samples with high crosslink density (5 min. UV exposure) were tested under 10 different strains starting with 14% to 3% and the measured crack size was plotted as a function of time (c). The same type of testing was conducted using PGSA samples with low crosslink density (15 sec. UV exposure) where the applied strains were adjusted based on the pre-determined critical strain starting with 21.5% to 16% and the measured crack size was plotted as a function of time (d). Note that linear fitting illustrated by the dashed lines was used to determine the crack growth rate for each of the applied strains in both cases discussed in c and d.

where H is the height of the sample, and the value of W was calculated by taking the area under the stress-strain curve of the un-notched sample from zero strain to the critical strain where the precut sample ruptures. By completing these calculations, we find that the fracture toughness values are equal to 19.56 J m $^{-2}$ and 14.78 J m $^{-2}$ for the high and low crosslink density PGSA, respectively (Table 1).

It is important to note that after 5 min of UV exposure, the cross-linking reaction is complete and no significant changes are observed when the sample is exposed to extended amounts of UV radiation. This can be clearly illustrated by conducting the same type of pure shear tensile testing using a PGSA sample that was exposed to 10 min of UV radiation and comparing the results. As seen in Figure 7c, the shear modulus of PGSA is unchanged after 5 min of UV exposure along with the cross-link density.

Based on the results collected from Figure 7 and Table 1, we know that by preparing samples using 5 min and 15 s of

UV exposure sufficiently allows us to produce two mechanically distinct PGSA samples. Because of that, we believe that the two samples should respond differently when exposed to similar experimental conditions. Therefore, and to confirm our hypothesis, we investigate the phenomena of SCC on both samples and compare the results in the remaining sections.

3.2.2. Experimental Setup for the Stress Corrosion Cracking Experiment

To study the SCC phenomenon in PGSA, and following the previous article, ^[5] we design a notched sample with the dimensions shown in **Figure 8**a where 1 cm from both ends is attached to an acrylate plate so that only 1 cm of the sample's width is exposed to testing conditions.

Table 2. Applied strain values, energy release rate, and crack velocity of high cross-link density PGSA exposed to 5 min of UV radiation along with the standard deviation values based on three replicate samples.

High cross-link density PGSA—5 min UV exposure			
Applied strain	Energy release rate [G, J m ⁻²]	Crack velocity [V, m s ⁻¹]	
14	16.55	$4.91 \pm 0.113 \times 10^{-5}$	
13	14.38	$3.87 \pm 0.098 \times 10^{-5}$	
12	12.31	$8.33 \pm 0.014 \times 10^{-5}$	
11	10.39	$2.75 \pm 0.007 \times 10^{-5}$	
10	8.64	$3.80 \pm 0.098 \times 10^{-5}$	
)	7.02	$4.13 \pm 0.049 \times 10^{-6}$	
3	5.56	$1.92 \pm 0.056 \times 10^{-5}$	
7	4.32	$4.67 \pm 0.002 \times 10^{-7}$	
5	3.18	$3.67 \pm 0.004 \times 10^{-7}$	
3	0.81	$3.33 \pm 0.003 \times 10^{-8}$	

The bottom acrylate plate is attached to an in-house designed water tank and the top plate is attached to the Instron's 10 N load cell (Figure 8b). Once in place, the tank is filled with DI water (pH 7) fully immersing the sample in solution. After that, ten different strain values that range from 14% to 3% for the high cross-link density PGSA are applied at 0.25% s⁻¹ ($\epsilon_{applied}$ < $\epsilon_{critical}$) and held constant for 3 hours or until crack propagation is complete (Figure 8b). The same type of testing was done using low crosslink density PGSA where the ten different strain values ranged from 21.5% to 16%.

To accurately measure the crack growth throughout the experiment, we used a high-resolution camera where images were captured periodically from time equals zero until the end of the experiment. The captured images were used to calculate the crack growth as a function of time that is then used to determine how the crack growth rate changes as a function of the applied strain.

3.2.3. Time-Dependent Crack Growth in the Sample with a Constant Strain

In Figure 8c, we plot crack size as a function of time based on the data collected from all 10 experiments using high crosslink density PGSA. We observe two regions of crack growth rates: high and low rates that are dependent on the applied strain. When the $\epsilon_{applied}$ values ranged from 14% to 8%, we observed rapid crack growth and full crack propagation within 2000 s or less. However, when the strain range is between 7% and 3%, we observe minimal crack growth with negligible propagation even after 3 h of constant strain application.

In the high crack growth rate region (Figure 8c), the crack velocity ranged from 4.91×10^{-5} to 1.92×10^{-5} m s⁻¹ for the 14% and 8% applied strain, respectively (Table 2). On the other hand, in the low crack growth rate region, the velocity was as low as 4.67×10^{-7} and 3.33×10^{-8} m s⁻¹ for the 7% and 3% applied strains, respectively (Table 2).

Similarly, in Figure 8d, we plot crack size as a function of time based on the data collected from all 10 experiments using low crosslink density PGSA. As is the case for the stiff PGSA sam-

Table 3. Applied strain values, energy release rate, and crack velocity of low cross-link density PGSA exposed to 15 s of UV radiation along with the standard deviation values based on three tested samples.

Low crosslink density PGSA—15 s UV exposure				
Applied strain	Energy release rate [G, J m ⁻²]	Crack velocity [V, m s ⁻¹]		
21.5	14.47	$2.93 \pm 0.035 \times 10^{-5}$		
21	13.82	$4.33 \pm 0.028 \times 10^{-5}$		
20.5	13.25	$3.88 \pm 0.014 \times 10^{-5}$		
20	12.64	$5.91 \pm 0.084 \times 10^{-5}$		
19	11.47	$2.03 \pm 0.063 \times 10^{-5}$		
18.5	10.88	$5.10 \pm 0.084 \times 10^{-5}$		
18	10.28	$1.25 \pm 0.024 \times 10^{-6}$		
17	9.23	$1.00 \pm 0.031 \times 10^{-7}$		
16.5	8.74	$4.00 \pm 0.00042 \times 10^{-7}$		
16	8.23	$1.67 \pm 0.034 \times 10^{-7}$		

ples, we also observe both low and high crack growth rate regions. When the applied strain ranges from 21.5% to 18.5%, the crack grows rapidly, and full propagation is observed within 2000 s or less. However, when the strain values ranged from 18% to 16%, slow to minimal crack growth was observed with negligible propagation within 3 h of the applied strain.

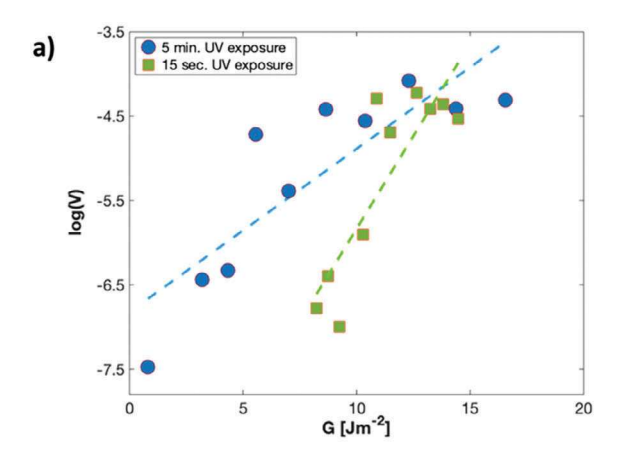
In the high crack growth rate region (Figure 8d), the crack velocity ranged from 5.91×10^{-5} to 2.03×10^{-5} m s⁻¹ for 20% and 19% strain, respectively (Table 3). In contrast, in the low crack growth rate region, the velocity ranged from 1.25×10^{-6} to 1×10^{-7} m s⁻¹ for 18% and 17% applied strains, respectively (Table 3).

Collectively, our results confirm that the crack growth rate increases as a function of the applied strain for both types of PGSA samples. We also confirm that the application of strain values that are close to the fracture strain accelerates crack growth and allow full propagation through the sample. Conversely, we strongly believe that in both cases when low strain values are applied on the sample, polymer hydrolysis on the surface of the crack becomes the prevailing factor that drives crack growth and is therefore significantly slower when compared to strain-driven crack growth.

3.2.4. Crack Growth Rate Versus Energy Release Rate

With the results that we have collected and discussed in the previous section, we can find a direct correlation between the crack growth rate, the applied strain, and their significant influence on the hydrolytic degradation of PGSA. By applying ten different strains on both types of PGSA, we apply a range of energy release rate (G in I m⁻²) values that are all less than the measured fracture toughness.

For example, in the case of high crosslink density PGSA with $\Gamma = 19.56 \text{ J m}^{-2}$, we apply a maximum G of 16.55 J m⁻² that was determined using Equation 2 and by calculating the area under the stress-strain curve of the un-notched sample using $\epsilon_{\it critical}$ that is equal to 14% strain. Similarly, and by using Equation 2, the energy release rate values applied on the high crosslink density PGSA ranged from 0.81 to 16.55 J m⁻² (Table 2). In the case of



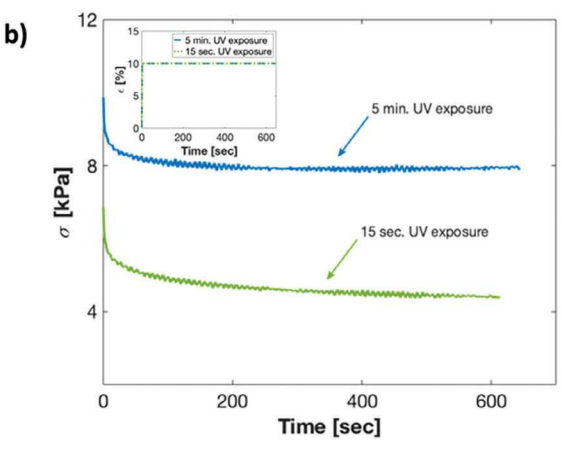


Figure 9. The logarithmic values of crack growth velocity in m s⁻¹ (V) were plotted as a function of the energy release rate in J m⁻² (G) for both the low and high crosslink density PGSA samples (a). Through linear fitting illustrated by the dashed lines, we observed that the initial velocity (V_0) changes with crosslink density. Therefore, we conducted a stress relaxation test under the same experimental conditions using the 10 N load cell to apply a 10% strain at 5% s⁻¹ where the strain was held constant for 10 minutes. The resulting stress was plotted as function of time (b). Our results confirm that under the same constant strain, the low crosslink density sample experiences larger % of stress relaxation when compared to the high crosslink density sample where the strain versus time results were added as an inset for the reader's reference.

low crosslink density PGSA, the values of G ranged from 8.23 to 14.47 J m $^{-2}$ (Table 3). To visualize how the crack growth rate is correlated with the applied energy release rate (G), we plot the logarithmic values of crack growth velocity (V) in m s $^{-1}$ as a function of the calculated energy release rate for both low and high crosslink density PGSA (**Figure 9a**). When both types of PGSA are exposed to high G values, the crack grows rapidly and prevails over the effect of hydrolytic degradation. However, when the applied G values are low, the two types of PGSA begin to exhibit different behavior as seen in Figure 9a.

We next aim to develop a quantitative understanding of the relationship between the crack growth rate and the applied energy release rate. Following, [4] we have:

$$\log V = \log V_0 - G\left(\frac{A^*}{K_B T}\right) \tag{3}$$

where V is the crack velocity, V_0 is the crack velocity when the energy release is zero, A^* is the activation area, K_B is Boltzmann's constant (1.38 × 10^{-23} J K⁻¹), and T is the absolute temperature (300 K). In the case of high cross-link density PGSA and using linear fitting (dashed line in Figure 9a), we find that the slope is equal to 0.181 m² J⁻¹ while the γ -intercept is equal to -6.692. By using Equation 3 along with the values obtained from linear fitting, we find that $V_0 = 2.03 \times 10^{-7}$ m s⁻¹ while $A^* = 7.50 \times 10^{-22}$ m² for high crosslink density PGSA.

Now, we can calculate the dissociation energy E_a as follows:

$$V_0 = a\nu * \exp\left(\frac{E_a}{K_B T}\right) \tag{4}$$

where ν is the average atomic frequency that is equal to 10^{14} Hz and a is the distance of the advancement of the crack tip with the breakage of an ester bond, which can be estimated by the mesh size and is approximately equal to 1 nm for PGSA based on the value of its modulus from Table 1. Based on these values, we find that under the influence of hydrolytic degradation, the dissociation energy E_a of the ester bonds in PGSA is equal to 29.14 kJ mol⁻¹ which is comparable to the values of ester bond dissociation energies reported in literature that range from 27.19 to 30.12 kJ mol⁻¹. [^{28,29}]

By applying the same type of linear fitting on the low crosslink density PGSA, we find that the value of V_0 is equal to 8.7×10^{-11} m s⁻¹ which is four orders of magnitude slower. This difference in the crack growth velocities can be explained by investigating the stress relaxation behavior of both types of PGSA where the same experimental setup discussed in Section 3.2.2 was used to apply a constant 10% strain on both samples at a rate of 5% s⁻¹. Within the first 10 min of the experiment (Figure 9b), we see that the stress relaxation in the PGSA with lower crosslink density is more significant (i.e., a larger percentage of stress relaxation). Therefore, during the SCC experiment, with a fixed strain, the true energy release rate applied to the elastomer actually decreases with time during crack growth, and the reduction of the energy release rate is greater for the PGSA with lower crosslink density. We believe the slow crack growth observed in PGSA with lower cross-link density is mainly because of its more significant stress relaxation.

4. Conclusions

With the rising concerns regarding global plastic pollution, degradable polymers offer a sustainable solution. However, during the degradation, breakdown of the polymer chains causes them to lose their mechanical strength and structural integrity which needs to be carefully studied for their practical applications. In the current work, we have investigated the hydrolytic erosion of PGSA, a photocurable and biocompatible elastomer, under various experimental conditions. By observing the in-situ degradation of PGSA in an aqueous environment, we confirm that the elastomer undergoes surface erosion. Moreover, the application of varying stress and strain values dramatically alters the degradation rate of the polymer. Our detailed investigations of the stress corrosion cracking phenomenon in PGSA have allowed us to understand the quantitative impact of the energy release rate and network relaxation on the crack growth rate of PGSA. Our

www.advancedsciencenews.com

- Chemistry and Physics
www.mcp-journal.de

[5] M. Shi, J. Steck, X. Yang, G. Zhang, J. Yin, Z. Suo, Extreme Mech. Lett. 2020, 40, 100978.

- [6] R. A. Gross, B. Kalra, Science 2002, 297, 803.
- [7] S. Walker, J. Rueben, T. V. Volkenburg, S. Hemleben, C. Grimm, J. Simonsen, Y. Mengüç, Int. J. Intell. Robot Appl. 2017, 1, 124.
- [8] J. Muller, C. González-Martínez, A. Chiralt, Materials 2017, 10, 952.
- [9] Science to enable sustainable plastics, Royal Society of Chemistry, a white paper from the 8th chemical sciences and society summit (CS3). 2020.
- [10] N. Lakshmi, C. Laurencin, Prog. Polym. Sci. 2007, 32, 762.
- [11] A. Göpferich, The Biomaterials: Silver Jubilee Compendium 1996, 117.
- [12] L. Suping, R. Sparer, D. Untereker, J. Polym. Sci., Part B: Polym. Phys. 2005, 43, 383.
- [13] A. Göpferich, Macromolecules 1997, 30, 2598.
- [14] J. A. Tamada, R. Langer, Proc. Natl. Acad. Sci. USA 1993, 90, 552.
- [15] F. Haynie, W. Boyd, Stress-corrosion Cracking of Aluminum Alloys, Springer, Cham, Switzerland 1966.
- [16] K. Sieradzki, R. Newman, Philos. Mag. A 1985, 51, 95.
- [17] M. Braden, A. N. Gent, J. Appl. Polym. Sci. 1960, 3, 90.
- [18] X. Yang, J. Yang, L. Chen, Z. Suo, Extreme Mech. Lett. 2019, 31, 100531.
- [19] M. Shi, Q. Jiao, T. Yin, J. J. Vlassak, Z. Suo, MRS Bull. 2023, 48, 45.
- [20] L. Vogt, F. Ruther, S. Salehi, A. R. Boccaccini, Adv. Healthcare Mater. 2021, 10, 2002026.
- [21] D. Sha, Z. Wu, J. Zhang, Y. Ma, Z. Yang, Y. Yuan, Eur. Polym. J. 2021, 161, 110830.
- [22] Y. Wang, G. A. Ameer, B. J. Sheppard, R. Langer, Nat. Biotechnol. 2002, 20, 602.
- [23] S. Gerecht, S. A. Townsend, H. Pressler, H. Zhu, C. L. E. Nijst, J. P. Bruggeman, J. W. Nichol, R. Langer, *Biomaterials* 2007, 28, 4826.
- [24] W. Yadong, Y. Kim, R. Langer, J. Biomed. Mater. Res. A 2003, 66, 192.
- [25] W.-S. Ao-leong, S.-T. Chien, W.-C. Jiang, S.-F. Yet, J. Wang, *Polymers* 2021, 13, 1960.
- [26] C.-T. Chang, H.-T. Chen, S. P. Girsang, Y. Chen, D. Wan, S.-H. Shen, J. Wang, Appl. Mater. Today 2020, 20, 100771.
- [27] J. Chen, J. Hwang, W.-S. Ao-leong, Y.-C. Lin, Y. Hsieh, Y.-L. Cheng, J. Wang, *Polymers* 2018, 10, 1263.
- [28] C.-G. Zhan, D. W. Landry, R. L. Ornstein, J. Am. Chem. Soc. 2000, 122, 2621.
- [29] H. Li, H. Li, Q. Dai, H. Li, J. Bredas, Adv Theory Simul 2018, 1, 1700015.

often outruns the surface erosion while uncovering how the applied energy release rate can quantitatively affect the degradation-induced crack growth rate in degradable polymers such as PGSA.

experimental results have demonstrated that hydrolytic cracking

Acknowledgements

The authors acknowledge the support by the NSF through grant no. CMMI-2029145 and the Saudi Aramco Advanced Degree Fellowship Program.

Conflict of Interest

The authors declare no conflict of interest.

Data Availability Statement

The data that support the findings of this study are available from the corresponding author upon reasonable request.

Keywords

degradable elastomer, energy release rate, ester bond dissociation energy, hydrolytic degradation, stress corrosion cracking, surface erosion

Received: August 26, 2023 Revised: December 6, 2023 Published online: December 20, 2023

- [1] V. Siracusa, P. Rocculi, S. Romani, M. Dalla Rosa, *Trends Food Sci. Technol.* **2008**, *19*, 634.
- [2] Plastics: Material-Specific Data, United States Environmental Protection Agency, 2017.
- [3] I. Vroman, L. Tighzert, Materials 2009, 2, 307.

Macromol. Chem. Phys. 2024, 225, 2300268

[4] Q. Jiao, M. Shi, T. Yin, Z. Suo, J. J. Vlassak, Extreme Mech. Lett. 2021, 48, 101433.